Progress In Electromagnetics Research C, Vol. 121, 221–232, 2022

Dual-Band Semi-Hexagonal Slot Antenna Backed by SIW for WLAN/WBAN Applications

Devabhaktuni Madhavi and Jagadeesh Dokuparthi*

Abstract—A hexagonal cavity backed antenna based on HMSIW is proposed to operate at 5.2 GHz and 5.8 GHz frequencies. The TM_{010} and TM_{110} modes of the hexagonal cavity resonator have been chosen to excite the structure. Afterwards, an HMSIW hexagonal cavity is formed by splitting conventional hexagonal cavity resonator along a magnetic wall. This enables a 50% reduction in size without affecting the antenna operating frequency. A rectangular slot is etched at the centre of the magnetic wall to curtail TM_{110} mode operating frequency. The dimensions of the slot are optimized to adapt TM_{110} resonant frequency to the desired frequency. In free space, the resulting antenna accomplished a peak gain of 5.5 dB and 4.3 dB at centre frequencies of 5.2 GHz and 5.8 GHz, respectively. In the vicinity of pork tissues, the antenna exhibits a peak gain of 4 dB at 5.8 GHz along with an efficiency of 87.2%.

1. INTRODUCTION

The latest wireless communication systems demand antennas that have high power handling capability, compact size, and low loss. Substrate Integrated Waveguide (SIW) is capable of handling high power and Q-factor while maintaining planar structure. Also, it has the ability to miniaturize the size without affecting the operating frequency. When the conventional SIW cavity is chopped by the side of a magnetic wall, a size reduction of 50% can be achieved. The resultant structure is named as Half Mode Substrate Integrated Waveguide (HMSIW). An HMSIW antenna designed using fundamental mode is proposed [1]. It achieves approximately 50% size reduction and radiates electromagnetic wave through dielectric aperture. Since the cavity backed antennas exhibit a unidirectional radiation pattern, they are more reliable for on-body applications. Most of the SIW cavity backed antennas are developed from rectangular [1] or circular [2] structures. Very few of the antennas are developed from hexagonal structure since the exact design equations for the cavity is not available. The expression for fundamental frequency of hexagonal SIW cavity was proposed in [3] in which approximate expression for the fundamental resonant frequency was reported. Later, a couple of SIW antennas based on a hexagonal structure was developed [4–9]. Hexagonal SIW cavity carries the benefits of circular cavity such as high Q-factor and provides more compact structures than circular SIW cavity when there is a requirement to design array antennas.

A dual band SIW cavity with two hexagonal slots [4] is excited using TM_{110} and TM_{210} modes to radiate the wave in the C-band. A rectangular antenna backed by HMSIW cavity with a semi-hexagonal slot [10] is developed for on-body applications. The semi-hexagonal slot is engraved on upper layer, shifted up the operating frequency of the antenna that leads to increase the size of the antenna. An SIW antenna developed on textile material for wearable applications [11] has achieved Specific Absorption Rate (SAR) of 0.9 W/kg. Several SIW antennas have been developed with the aid of semi-circular slot [12], circular ring slot [13], rectangular ring slot [14] to accomplish unidirectional radiation pattern.

Received 26 May 2022, Accepted 7 June 2022, Scheduled 25 July 2022

* Corresponding author: Jagadeesh Dokuparthi (d_jagadish4@yahoo.co.in).
The authors are with the R. V. R. & J. C. College of Engineering, Chowdavaram, AP, India.

In this paper, a dual-band, compact SIW cavity backed slot antenna is proposed. HMSIW is employed in the proposed structure to accomplish compactness. The magnetic wall serves as a radiator which emits electromagnetic waves at first band. The slot etched on top of the structure has helped to bring the second resonance to the desired band and also causes an electromagnetic wave to emit at the second band.

2. ANTENNA STRUCTURE

A two side, copper coated substrate (RT Duroid-5880), with size of 30 mm × 21 mm, is selected to develop the proposed antenna. Several metallized vias are embedded into the material to shape a semi-hexagonal structure as shown in Figure 1. The structure is enclosed by a series of vias at three sides and kept open at one side (magnetic wall). The open structure helps to radiate EM waves from semi-hexagonal structure into free space. A slot is etched in perpendicular to the magnetic wall to bring the TM_{110} mode to the desired frequency. The structure is excited by co-axial feed which helps in achieving compact structure. The proposed structure geometrical parameters are exhibited in Table 1.

Table 1. The parameters of the proposed structure.

Parameter	L	ex	d	ds	Sl	w	fx	fy
Value (mm)	16.2	2.7	1.2	1.8	9.3	1	8	−9

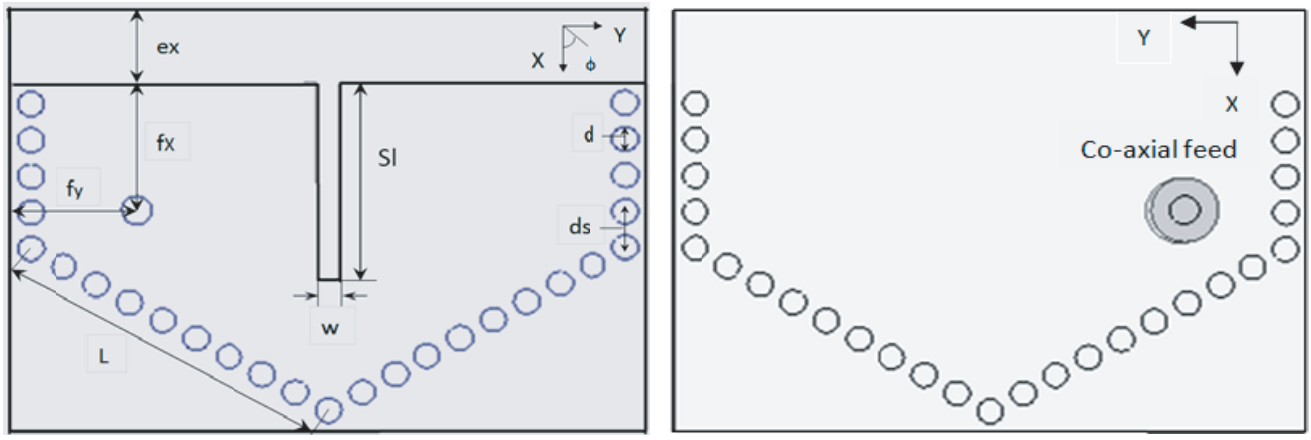

(a) (b)

Figure 1. Proposed antenna structure. (a) Upper layer view. (b) Bottom layer view.

3. ANTENNA DESIGN EVOLVEMENT

3.1. Design of Hexagonal HMSIW Antenna

The antenna design evolvement was initiated with the design of a regular hexagonal cavity resonator (HCR). Since there is no exact equation to design side length of HCR, the estimated formula is considered from [3]. The length of the regular HCR based on SIW is estimated such that the fundamental frequency is situated near 5 GHz frequency.

$$L^{SIW} = \frac{c\mu'}{2\pi f\sqrt{\epsilon_r}} \tag{1}$$

where 'L^{SIW}' is the regular HCR side length, 'ϵ_r' the dielectric constant of the substrate, 'c' the light velocity in free space, and $\mu' = 2.75$ the modified Bessel coefficient for fundamental frequency.

After designing HCR, it is partitioned into two parts. However, there is an aperture added at magnetic wall to support the radiation. One half of the partition of the HCR with aperture which is named as hexagonal HMSIW is used to develop the proposed structure.

The effective side length of hexagonal HMSIW structure is

$$L_{eff}^{HMSIW} = L^{SIW} + \Delta L \tag{2}$$

where ΔL is the change in length due to fringing fields at dielectric aperture which can be calculated using nonlinear least squares method [19, 20].

$$\Delta L = h\left(0.005+\frac{0.30}{\varepsilon_{reff}}\right)\times \ln\left(0.79\frac{L_{eff}}{4h^3}+\frac{52L_{eff}-261}{h^2}\frac{38}{h}+2.77\right) \tag{3}$$

$$\varepsilon_{reff} = \frac{\varepsilon_r+1}{2}+\frac{\varepsilon_r-1}{2}\left[1+12\frac{h}{L_{eff}}\right]^{\frac{-1}{2}} \tag{4}$$

Finally, a slot at the middle of the structure is placed to tune the resonant frequency of the TM_{110} mode.

3.2. Antenna Working Principle

Side length of the HCR is a major parameter which decides the frequencies of the resonant modes. The side length of the HCR is calculated from the above equations. The TM_{010} and TM_{110} modes of the HCR are used to excite the proposed structure. Figure 3 shows that the E-field distribution of the modes are symmetric about the Y-axis. Hence, they can be halved along the middle line without affecting operating frequencies and field distributions. Next, a slot is etched to bring down the resonant frequency of the TM_{110} mode. The position of the slot is selected such that it disturbs the current distribution of the TM_{110} mode alone. This phenomenon enables the structure to tune the TM_{110} mode independently. Otherwise, the insertion of slot alters both the resonant modes. When the resulted structure is excited using co-axial feed, it radiates through dielectric aperture at lower resonant frequency (5.2 GHz) and slot at upper resonant frequency (5.8 GHz).

3.3. Simulation Results

The Full Mode HCR designed using the above equation is simulated using HFSS. The simulated reflection coefficient of FMHCR shows that the fundamental mode (TM_{010}) and next higher order mode (TM_{110}) are situated at 5.3 GHz and 8.8 GHz, respectively. The E-field and surface current densities of the above modes are exhibited in Figure 3.

The line OP shown in Figure 2 is symmetric about the Y-axis and passes through the maximum E-field of both the TM modes. Hence, the structure can be cut into two pieces for miniaturization. The remaining part of the structure with dielectric aperture is shown in Figure 3(b). The E-field and current densities of the semi-hexagon-shaped HMSIW cavity is exhibited in Figure 4. There exists a slight change in the resonant frequencies of both the modes due to the existence of fringing fields at the dielectric aperture. The simulated resonant frequencies of the hexagonal HMSIW cavity reach 5.2 GHz and 8.71 GHz for the TM_{010} and TM_{110} modes, respectively. The current flowing on the top layer of the structure can be perturbed through insertion of the slot. Figures 4(c) & 4(d) explain that the current situated at the center (along X-axis) of the HMSIW cavity is minimum for TM_{010} mode and maximum for TM_{110} mode, respectively. By introducing a slot at the center, the current at the TM_{110} mode can be perturbed as a result of the path taken by the current increases. The enlargement in current displacement causes an increase in the inductance of the structure at TM_{110} mode. This phenomenon helps to lower the structure resonant frequency at TM_{110} mode. TM_{110} mode is shifted from 8.71 GHz to 5.8 GHz frequency by etching a slot at the middle of the structure as shown in Figure 2(c). The fundamental mode (TM_{010}) resonant frequency is not significantly affected by the slot since the current distribution at the slot location is minimum. Thus, only TM_{110} mode resonant frequency is altered by etching the slot.

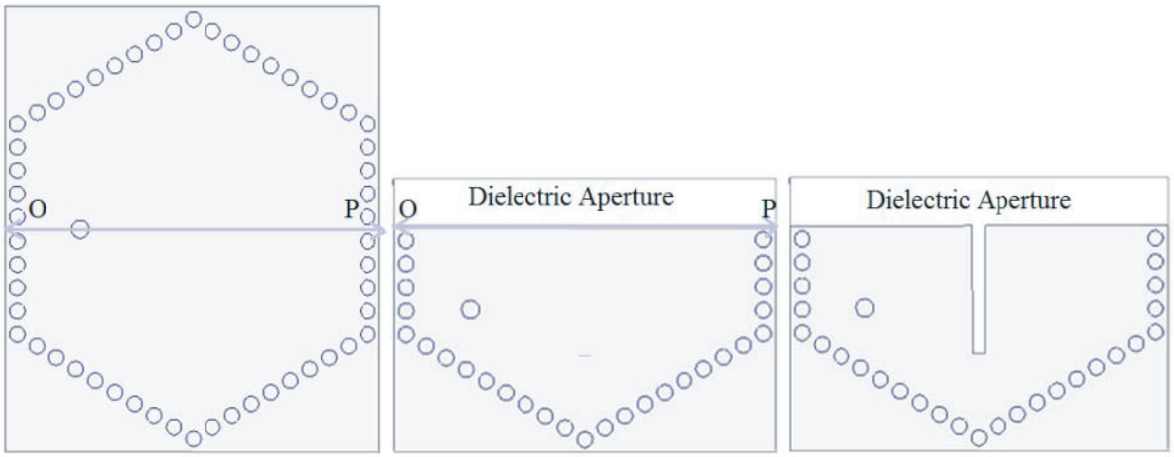

Figure 2. Design evolvement of proposed antenna. (a) Full Mode Hexagonal SIW Cavity. (b) HMSIW Hexagonal cavity. (c) HMSIW Hexagonal cavity with slot (Proposed Structure).

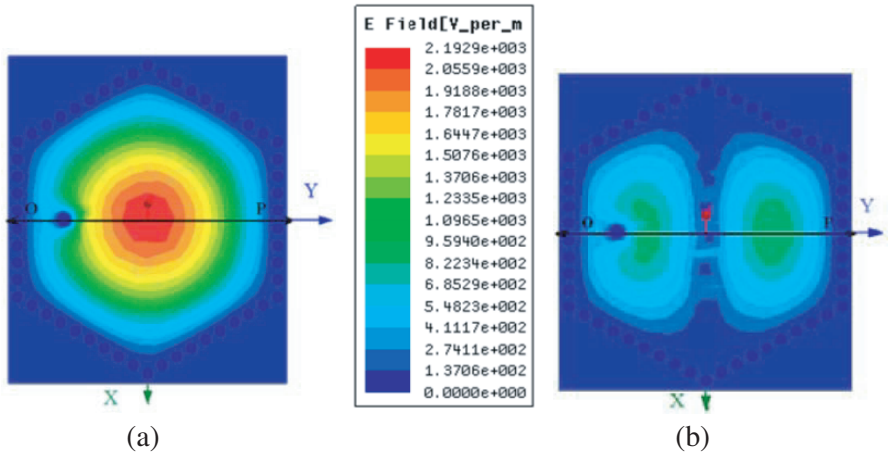

Figure 3. E-field densities of the Full Mode Hexagonal SIW cavity at (a) 5.3 GHz: TM_{010} mode, (b) 8.8 GHz: TM_{110} mode.

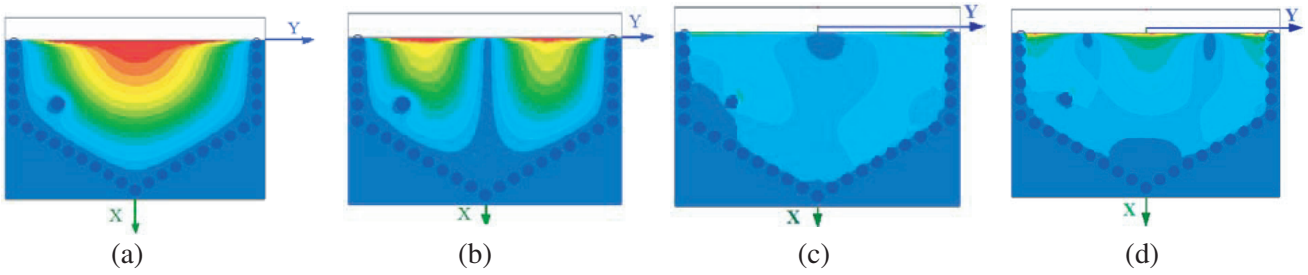

Figure 4. E-field densities of HMSIW HCR at (a) 5.2 GHz, (b) 8.71 GHz, Current densities of HMSIW Hexagonal cavity at (c) 5.2 GHz, (d) 8.71 GHz.

4. PARAMETRIC ANALYSIS

4.1. Selection of Feed Location

To achieve good impedance matching, the feed position of the HMSIW structure is optimized. A diagonal line has been drawn to study the impedance of the structure at various positions. The

impedance at point 'A' is near zero since the point is close to metallized vias (PEC wall). As the metallized vias behave like a short circuit, the voltage across them is zero, and the current through them is maximum. Hence, the impedance in the location reaches zero. In contrast, the impedance at point 'D' is close to infinite since the point almost reaches open ended terminal. As the open ended terminal voltage is maximum and current near zero, the impedance offered by the point reaches infinity. To match input impedance of the structure to SMA connector whose impedance is 50 Ω, the parametric analysis has been performed near point 'A'. Thus, the feed location of the antenna between points 'B' and 'C' yields good impedance matching. The reflection coefficient of the HMSIW structure by varying feed position between points 'B' and 'C' is presented in Figure 5. It depicts that the HMSIW structure accomplishes good impedance matching when the feed is located at $(fx, fy) = (8\,\text{mm}, -9\,\text{mm})$ from the centre along the line AD as shown in Figure 5.

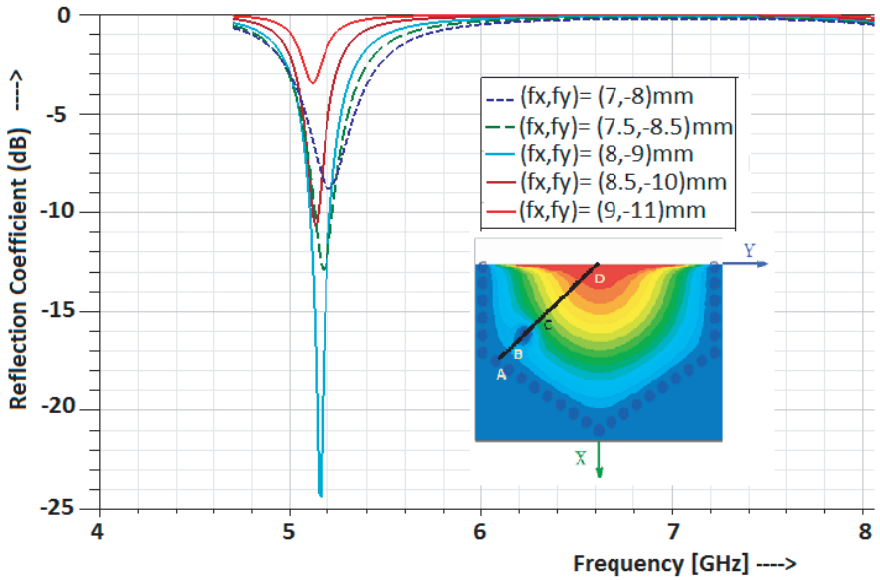

Figure 5. Variation of reflection coefficient with feed location.

4.2. Effect of Slot at Middle

The primary parameter for tuning the resonant frequency of TM_{110} mode is slot length. Parametric analysis shown in Figure 6 explicates that the resonant frequency reaches 5.8 GHz when the slot length is changed to 10 mm. It is also observed that the slot only affects TM_{110} mode. There is no significant effect on TM_{010} mode since the current density of the mode at slot position is minimum. The figure also shows that there is a negligible effect on S_{11} of TM_{010}. Thus, the resonant frequency of the slot is tuned from 8.75 GHz to 5.8 GHz by varying the slot length from 0 to 10 mm. The Frequency Ratio (FR) of the design due to middle slot variation ranges from $f_H/f_L = 1.11$ to 1.44 when $|S_{11}| < -10$ dB is considered.

4.3. Effect of Dielectric Aperture

The increase in width of the dielectric aperture improves the performance of the antenna. Since there is a direct proportion between the gain and aperture of the antenna, the gain of the antenna is improved with increasing dielectric aperture width. Figure 7 explicates that the gain of the antenna is enhanced with icreased width of the dielectric aperture. The gain increases significantly while the aperture width is increased to 3.5 mm. To accomplish a perfect unidirectional radiation pattern, the antenna Front to Back Ratio (FTBR) should be high. When the width of the dielectric aperture is increased, the ground plane which appears below the dielectric aperture also increases. The increase in length of the ground

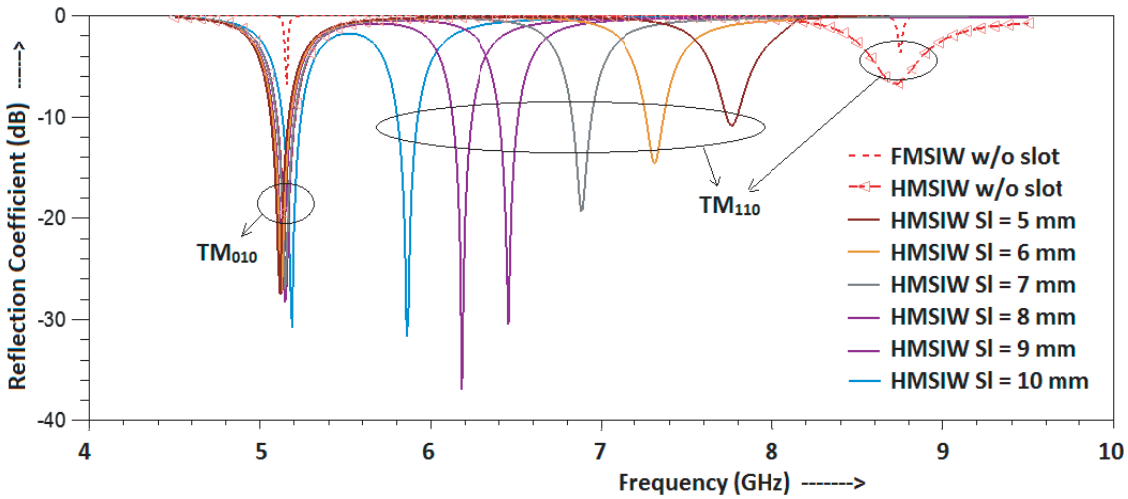

Figure 6. Effect of slot length on reflection coefficient.

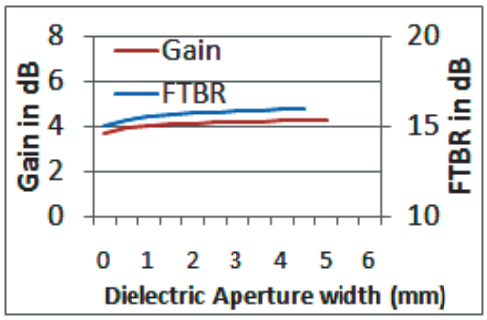

Figure 7. Effect of Dielectric aperture on Gain and FTBR.

layer prevents the back radiation. Thus, the FTBR is also improved with increasing the width of the dielectric aperture.

5. DISCUSSION ON RESULTS

5.1. Radiation Mechanism of Proposed Structure

The proposed structure operates in dual bands in which the 1st band centre frequency is 5.19 GHz while 5.83 GHz is the 2nd band centre frequency. The current density plot shown in Figure 8(a) elucidates that the maximum of current is located along the dielectric aperture at 5.19 GHz frequency. Also, the plot in Figure 8(c) shows that the E-field is situated along the dielectric aperture. Thus, the EM wave is emanated into the far-field from the dielectric aperture with maximum E-field along the X-axis. The current density at 5.83 GHz is exhibited in Figure 8(b) which indicates that the maximal current is located over the slot. Also, the plot shown in Figure 8(d) displays that the maximal E-field is located in the slot. Since the electric field within the slot exists along its width, the E-field at 2nd band directs along the Y-axis. Thus, the EM wave is radiated into the far-field through the slot with maximal E-field along the Y-axis.

5.2. Discussion on Measured Results

The prototype photograph of the proposed structure is exhibited in Figure 9. The $|S_{11}|$ of the proposed structure is assessed with the aid of Anritsu Vector Network Analyzer (VNA). The simulated and

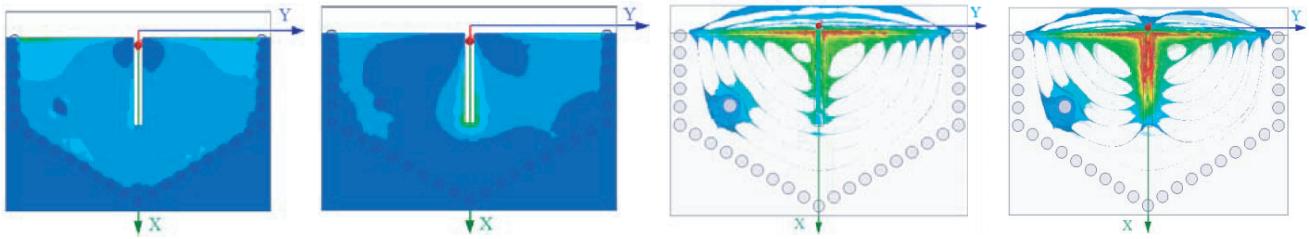

Figure 8. Surface current density at (a) 5.19 GHz and (b) 5.83 GHz, E-field density at (c) 5.19 GHz and (d) 5.83 GHz.

Figure 9. (a) Top View of the Proposed Antenna prototype, (b) S_{11} measurement setup of proposed antenna.

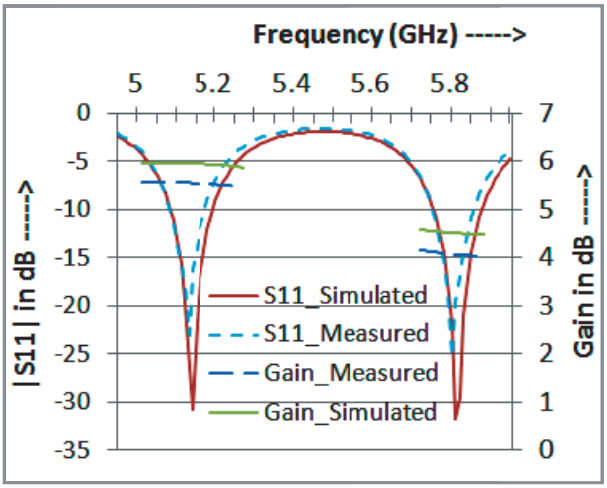

Figure 10. Comparison of simulated and experimental results of $|S_{11}|$ and Gain.

experimental results exhibited in Figure 10 elucidate that the antenna centre frequencies are situated at 5.2 GHz and 5.8 GHz. In free space, the measured operating frequency ranges from 5.145 to 5.255 GHz at band1 while it is from 5.76 to 5.845 GHz at band2.

The proposed antenna excited by lumped port is simulated in Ansys HFSS software. The radiation boundary is kept $\lambda/3$ distance away from the antenna edges. Figure 11 delineates the radiation plots

of the proposed antenna at the centre frequencies of two operating bands. The normalized radiation plots of E & H-planes at 5.2 GHz frequency are exhibited in Figures 11(a) & (b), respectively. The figures witness that the antenna exhibits perfect unidirectional radiation pattern as its FTBR reaches 30 dB. The peak Cross Polarization Level (CPL) is 19 dB lower than the required polarization level at boresight direction in both the planes. Figures 11(c) & (d) depict the E & H-plane normalized plots at 5.8 GHz frequency. The FTBR and peak CPL are 16 dB and 18 dB, respectively.

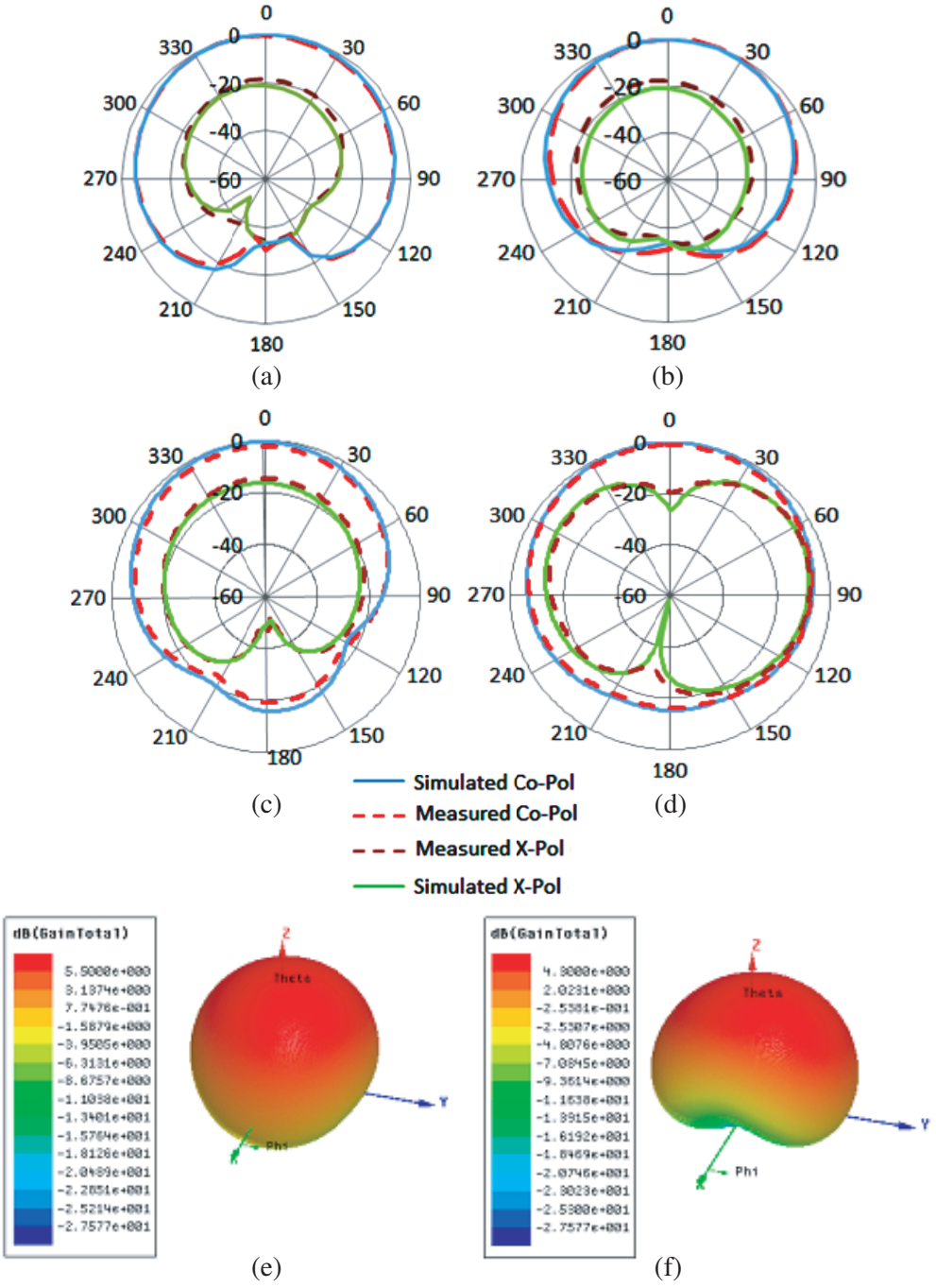

Figure 11. Normalized radiation patterns of 1st band, (a) E-plane, (b) H-plane, and, 2nd band (c) E-plane, (d) H-plane, (e) 3-D radiation plot at 1st band centre frequency, (f) 3-D radiation plot at 2nd band centre frequency.

5.3. Simulation on Phantom Model

In the simulation, the proposed antenna performance is assessed in the vicinity of the phantom model (85 mm × 85 mm × 30 mm). Three layers are considered in the phantom model, skin, muscle, and fat, as shown in Figure 12. The properties of these layers [21], such as conductivity, permittivity, and loss tangent at 5.8 GHz frequency, are enumerated in Table 2. The proposed antenna is simulated in the vicinity of a phantom model to examine the SAR. The SAR of the proposed hexagonal HMSIW antenna is calculated on 1 g mass of tissue averaged over the density of 910 g/cm^3 with input power of 100 mW. The maximum SAR of the antenna is 638 mW/kg, 631 mW/kg, and 625 mW/kg when the proposed structure and phantom are separated by a distance of 2 mm, 3 mm, and 4 mm, respectively. Figure 12(a) depicts that more power is dissipated at the middle of the phantom model than other regions since the slot etched at the middle of the cavity is responsible for radiating EM wave. As the achieved SAR value is much lower than standard SAR of 1.6 W/kg, the proposed hexagonal HMSIW cavity back antenna is well suited for WBAN applications.

Table 2. Characteristics of body layers at 5.8 GHz.

Parameters	Skin	Fat	Muscle
Dielectric Constant	35.2	4.89	48.4
Loss Tangent	0.288	0.16	0.267
Conductivity (S/m)	3.75	0.33	4.85

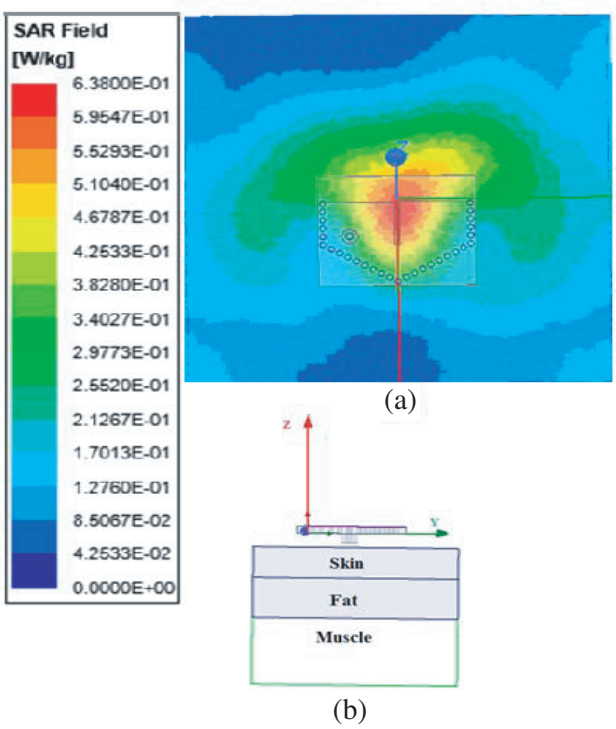

Figure 12. (a) SAR plot on Phantom model. (b) Schematic of the proposed structure with phantom model.

Figure 13 shows the $|S_{11}|$ and gain in dB in the vicinity of Phantom and Pork tissues. The reflection coefficient is shifted up at the two operating frequencies when the antenna is situated in the vicinity of the pork tissues owing to different material properties of the tissues. However, the reflection coefficient is well below −10 dB at the two operating frequencies that shows the proposed antenna is a strong candidate for on-body applications.

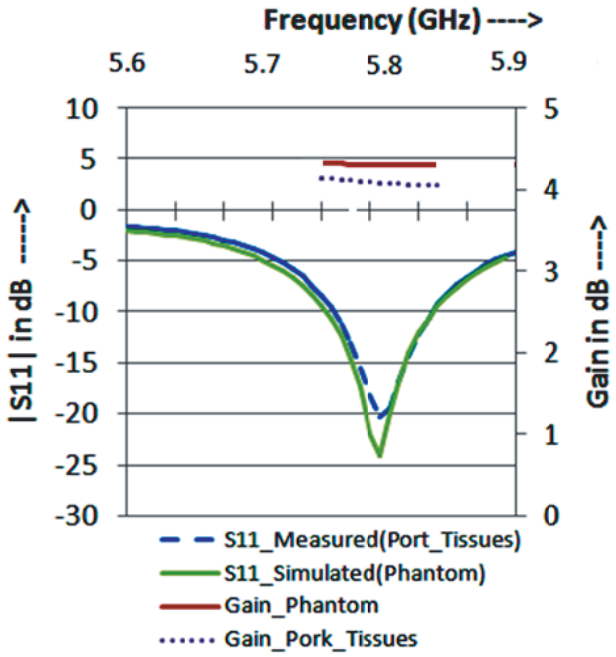

Figure 13. Gain and $|S_{11}|$ of the proposed antenna in the vicinity of Phantom and Pork tissues.

The radiation performance of the proposed structure in the vicinity of pork tissues is presented in Figure 14. It delineates that not much deviation is observed in the co-polar radiation pattern compared with free space condition. In cross-polar radiation pattern, a back lobe occurs in both the planes as there are pork tissues under the structure. This is attributed to different electromagnetic properties exhibited by the pork tissues.

The proposed antenna's performance is compared with reference antennas in Table 3. λ_l is the

Table 3. Comparison of Antenna performance with Ref. antennas.

Ref.	Antenna Size (λ_l^2)	Centre frequency (GHz)	Gain (dBi)	Fractional Impedance BW	Dielectric Constant	Thickness (mm)
[14]	0.147	2.4 5.8	2.13* 5.16*	1.25% 1.9%	2.33	0.019 λ_l
[15]	0.38	2.4 5.8	0.56* −1.59*	4.9% 2.8%	4.4	0.053 λ_l
[16]	0.849	8.8 11.3	5.3 4.3	2% 1.4%	2.2	0.034 λ_l
[17]	0.72	8.6 13.3	5.1 6.3	2.3% 6%	2.2	0.05λ_l
[18]	0.39	5.2 5.8	3.31 4.16	2.32% 2.4%	2.2	0.005λ_l
This Work	0.416	5.2 5.8	5.5 4.1*	1.73% 1.71%	2.2	0.005 λ_l

* indicates on-body results

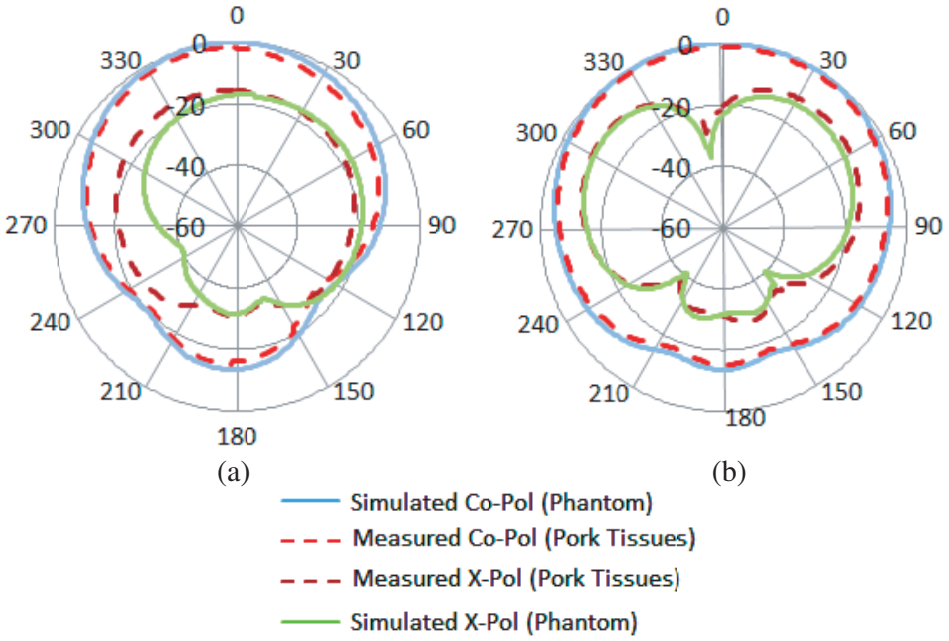

Figure 14. Normalized patterns in the vicinity of Phantom and pork tissues at 5.8 GH. (a) *E*-Plane. (b) *H*-Plane.

guided wavelength of the lowest operating frequency of the respective antenna. In Table 3, on-body results are shown for the proposed work and Refs. [14, 15]. Refs. [14, 15] provide compact size compared with the proposed work. However, the antenna in [14] suffer from poor cross polarization while the antenna in [15] renders low gain. The antennas developed in [16, 17] possess little improvement in gain. However, the size of the antennas [16, 17] approximately double the proposed design. Even though the antenna proposed in [18] offers slightly smaller size than present work, it cannot be operated simultaneously in both the bands.

6. CONCLUSION

In this paper, an HMSIW is designed, fabricated, and elucidated. The antenna performance is assessed both in free space and vicinity of the pork tissues at 5.8 GHz frequency. The measured results are in good agreement with simulated ones. The proposed antenna is a low profile, robust, and single layered structure, which is appropriate for WLAN/WBAN applications.

REFERENCES

1. Kumar, A., D. Chaturvedi, and S. Raghavan, "Design and experimental verification of dual-fed, self-diplexed cavity-backed slot antenna using HMSIW technique," *IET Microw. Antennas Propag.*, Vol. 13, No. 3, 380–385, 2019.
2. Kumar, A. and S. Raghavan, "A design of miniaturized half-mode SIW cavity backed antenna," *2016 IEEE Indian Antenna Week (IAW 2016)*, 4–7, 2016.
3. Xu, Z. Q., Y. Shi, P. Wang, J. X. Liao, and X. B. Wei, "Substrate Integrated Waveguide (SIW) filter with hexagonal resonator," *Journal of Electromagnetic Waves and Applications*, Vol. 26, No. 11–12, 1521–1527, 2012.
4. Sudhakar, A. and D. Jagadeesh, "Dual-band hexagonal cavity back slot antenna using TM_{110} and TM_{210} modes," *2019 Photonics & Electromagnetics Research Symposium — Fall (PIERS — FALL)*, Xiamen, China, December 17–20, 2019.

5. Liu, H., A. Qing, B. Wu, and Z. Xu, "Low-profile hexagonal SIW cavity slot antenna with enhanced gain by using quasi-TM_{310}] mode," *IET Microwaves, Antennas & Propagation*, Vol. 14, No. 7, 629–633, 2020.
6. Chaturvedi, D. and S. Raghavan, "A dual-band half-mode substrate integrated waveguide based antenna for WLAN/WBAN applications," *Int. J. RF Microw. Comput. Aided Eng.*, Vol. 28, No. 5, e21239, 2018.
7. Banerjee, S., S. Chatterjee, S. Das Mazumdar, S. Chakraborty, S. Bhattacharya, and M. Gangopadhyaya, "A compact half-mode SIW semi-hexagonal antenna with T-shaped slot," *2017 2nd International Conference for Convergence in Technology (I2CT)*, 2017.
8. Valizade, A., J. Nourinia, Ch. Ghobadi, and B. Mohammadi, "Compact HMSIW hexagonal cavity patch antenna," *2017 IEEE 4th International Conference on Knowledge-Based Engineering and Innovation (KBEI)*, Dec. 2017.
9. Banerjee, S., M. Debnath, S. Bose, D. Bhattacharya, R. A. Mondal, and P. Basu, "Compact HMSIW semi-hexagonal antennas with rectangular slot," *2019 International Conference on Opto-Electronics and Applied Optics (Optronix)*, 2019.
10. Chaturvedi, D. and S. Raghavan, "A half-mode SIW cavity-backed semi-hexagonal slot antenna for WBAN application," *IETE Journal of Research*, Vol. 65, No. 5, 582–588, 2018.
11. Agneessens, S. and H. Rogier, "Compact half diamond dual-band textile HMSIW on-body antenna," *IEEE Trans. on Antenn. and Propg.*, Vol. 62, No. 5, 2374–2381, May 2014.
12. Chaturvedi, D. and S. Raghavan, "Compact QMSIW based antennas for WLAN/WBAN applications," *Progress In Electromagnetics Research C*, Vol. 82, 145–153, 2018.
13. Hong, Y., J. Tak, and J. Choi, "An all-textile SIW cavity-backed circular ring-slot antenna for WBAN applications," *IEEE Antennas and Wireless Propagation Letters*, Vol. 15, 1995–1999, 2016.
14. Zhu, X., Y. Guo, and W. Wu, "A compact dualband antenna for wireless body-area network applications," *IEEE Antennas and Wireless Propagation Letters*, Vol. 15, 98–101, 2016.
15. Tak, J., S. Woo, J. Kwon, and J. Choi, "Dual-band dual-mode patch antenna for on-/off-body WBAN communications," *IEEE Antennas and Wireless Propagation Letters*, Vol. 15, 348–351, 2016.
16. Althuwayb, A. A., M. J. Al-Hasan, A. Kumar, and D. Chaturvedi, "Design of half-mode substrate integrated cavity inspired dual-band antenna", *Int. J. RF Microw. Comput. Aided Eng.*, Vol. 31, No. 2, e22520, 2020.
17. Kumar, A., M. Saravanakumar, and S. Raghavan, "Dual-frequency SIW-based cavity-backed antenna", *AEU — International Journal of Electronics and Communications*, Vol. 97, No. 1, 195–201, 2018.
18. Kumar, A., C. Divya, and S. Raghavan, "Design and experimental verification of dual-fed, self-diplexed cavity-backed slot antenna using HMSIW technique," *IET Microwaves, Antennas & Propagation*, Vol. 13, No. 3, 380–385, 2019.
19. Lai, Q., C. Fumeaus, W. Hong, and R. Vahldieck, "Characterization of the propagation properties of the half-mode substrate integrated waveguide," *IEEE Trans. Antennas Propag.*, Vol. 57, No. 8, 1996–2004, 2009.
20. *Numerical Analysis*, T. Sauer, Ed., Person Educ., Upper Saddle River, NJ, USA, 2006.
21. Means, D. L. and W. Kwok, "Evaluating compliance with FCC guidelines of human exposure to radiofrequency electromagnetic fields," *Federal Communications Commission Office of Engineering & Technology, Supplement C*, (edition 01-01) to OET Bulletin 65 (Edition 97-01), Jun. 2001.